Jet Propulsion Lab Report

C. Mollet, S. Vial, G. Borrelli, F. Steiner

December 2020

1 Introduction

Jet engines are the most common type of propulsion system in air transportation. Today, it is safe to assume that the vast majority of civil aviation is powered by turbofan engines, that rely on turbo machinery to operate. Considering the size of the sector, and in a context of cost and emissions reduction, the concept of efficiency is therefore of primary interest.

For every irreversible processes, losses are a central phenomenon, that can not be neglected. The turbomachinery behind a turbofan engine includes turbines, for which the losses result in a decrease of the extracted energy from the air flow, compared to the ideal isentropic process. In order to measure the losses in a turbine stage, experiments are usually done per row, which means that we obtain individual losses for the rotor and the stator.

Losses in a blade row of an annular turbine can be either profile losses, tip leaking losses or endwall losses. The three different types of losses are schematized in Figures 1 and 2.

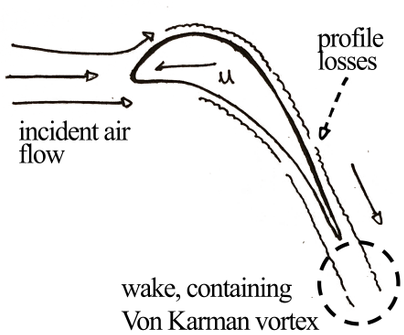

Figure 1: Profile losses.

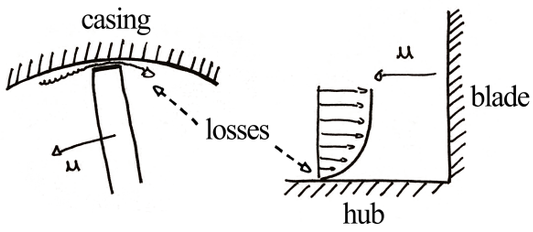

Figure 2: Tip leaking losses (left) and endwall losses (right).

The objective of this lab is to evaluate, by measurements, the loss coefficient for a turbine blade row. As explained further bellow, this experiment will be carried out on a linear non rotating cascade blade row, long enough to disregard the near-wall effects. Therefore, as we are also working on a non-annular row, tip leaking losses and end wall losses will be disregarded in this experiment, and we will focus on the profile losses.

The aerodynamic loss coefficient will be determined through experimental measures, based on probe transverse measurements. Different parameters, like the inlet angle and the surface roughness, will be modified, so that their influence is studied in the process. The following section will go through the experimental setup, and the sensors we used.

2 Experimental setup

2.1 Remote interface

Being not possible to be physically in the lab, the experiment has been conducted remotely.
On the remote interface (seen in Figure 3), it is possible to define the angle of the cascade with respect to the flow as shown on Figure 4. The other parameters are then the span-wise and pitch-wise range for the probe. For the measurements, the span-wise coordinate is fixed approximately in the middle of the span and several points are taken along the pitch to cover multiple blades. The pressure is then measured by the probe and, using the differences in pressure along the pitch, the loss coefficient can be measured and compared with Soderbergh's one.

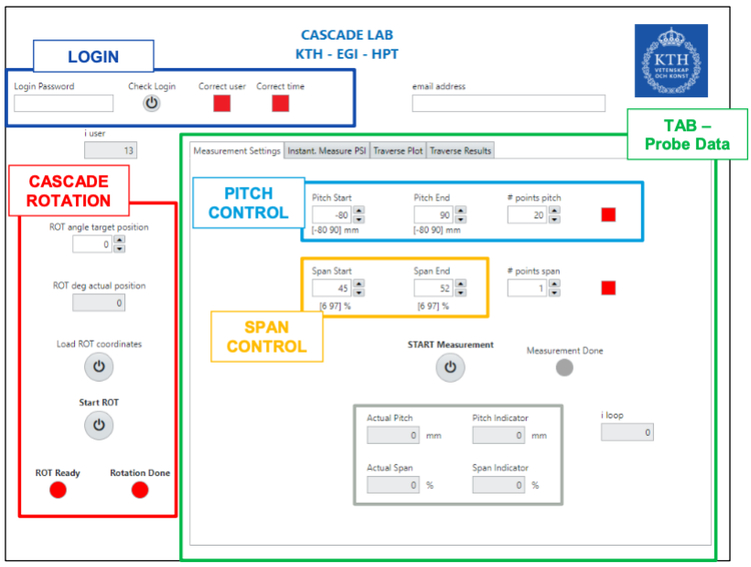

Figure 3: Illustration of the Remote Interface used for the experiment.

Once the first measurements are done, the **spatial resolution** and the influence of the **roughness** of the blades can be investigated.
The experiments will be conducted for the same conditions with a higher number of points in the pitch-wise direction, for the first case.
For the influence of the roughness, different blades are used. Those rougher blades can be selected if the *pitch start* is around -80 mm, as illustrated in Figure 3. The probe will then move up to those blades to start the pressure measurements.

Finally, the last experiment will require to modify the **inlet angle** at a given fan frequency using the ROT angle to see its influence on the pressure loss.

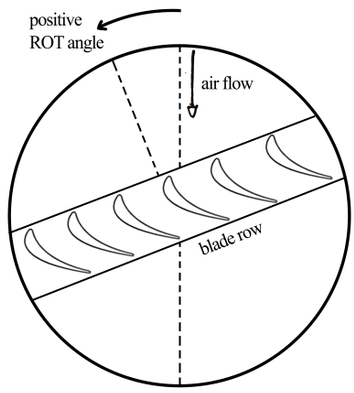

Figure 4: Simple model of the linear cascade in the open sub-sonic wind tunnel.

The rotation of the linear cascade in the wind tunnel can be modeled as in Figure 4, where the ROT angle was set to a positive value. It is important to relate the angle of rotation inside the web interface in order to obtain the desired stator inlet angle of the flow. As we have established in the course, the conventional direction to write the positive flow angles, is by putting the positive angles in the direction of the blade speed (usually denoted u). On Figure 5, if we were to draw the rotor after the stator, it would have a speed oriented downwards. Therefore, positive angles are the ones pointing downwards. By comparing carefully the Figures 4 and 5, we can see that the positive ROT angle corresponds in reality to a negative flow angle for the turbine stage.

2.2 Facility and Instrumentation

The experiment is performed at *subsonic* speed and the flow is generated thanks to an *open-type* wind tunnel. The air flowing through the facility moves from the inlet through the cascade and, finally, it is discharged in the surroundings.
The test rig is supplied by a 90 kW blower which allows to reach up to a Mach number of 0.4. The variable inlet angle ranges from $-30°$ to $+30°$.

In order to perform the measurements which are needed to evaluate the loss coefficient ζ, as described in the following section, the following instrumentation has been employed:

- Upstream: Total Pressure and Total Temperature measurement devices
- Downstream: 3-holes Aerodynamic Probe traverse

The role of the traversing system positioned downstream the cascade is crucial. The latter is, indeed, very relevant in the evaluation of the pressure's profile after the cascade, thus it allows to have an intuitive understanding of how losses behave (see graphs in the section related to the *Results*).
The three holes are positioned on a *wedge-shaped* probe in such a way that, together with the information related to the flow direction, also the total and static pressures are read: the edge oriented with a $0°$ angle in the outflow measures p_0, the remaining two holes the static p.
Without going too much into details, it is useful to point out that the type of measurement is performed, by means of a digital multi-channel pressure scanner, relatively to the atmospheric pressure. The 3-hole measurement requires to be calibrated, so to have a good mapping of the quantities of interest with respect to the variation of some parameters (e.g. Mach number, yaw angle..).
Finally, the total temperature is measured using a standard PT100 sensor.

3 Theoretical Background

3.1 Loss Coefficient Calculation

In the performed experiment, a flow through a *turbine* stator blade row (i.e. *cascade*) has been analysed. A schematic representation of the cascade is illustrated in Figure 5.

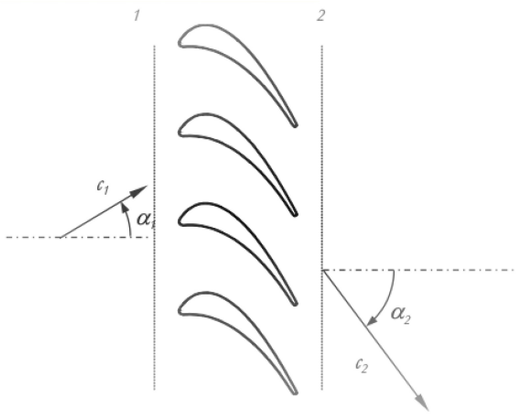

Figure 5: Turbine stator blade row.

Having a turbine, it is good to point out that the flow will accelerate, experiencing a pressure drop.
In the case of an ideal process, all the kinetic energy would be recovered. This doesn't apply to reality because this process is irreversible, thus it will account for losses (e.g. due to friction), leading to an increase of entropy.
As formula (1) states, the difference in enthalpy due to losses Δh_{loss} is linked to the absolute velocity at the stator's exit c_2 through a non-dimensional *loss coefficient* ζ.

$$\Delta h_{loss} = \zeta \frac{c_2^2}{2} \tag{1}$$

In order to determine this enthalpy difference, we can use the difference in terms of kinetic energies, as seen in the equation bellow:

$$\Delta h_{loss} = \frac{c_{2s}^2}{2} - \frac{c_2^2}{2} \tag{2}$$

The *loss coefficient* reads as:

$$\zeta = \frac{c_{2s}^2 - c_2^2}{c_2^2} \tag{3}$$

Here c_{2s}^2 is the kinetic energy obtained from the isentropic process and it is calculated as:

$$c_{2s}^2 = 2c_p(T_{01} - T_{2s}) \tag{4}$$

The outlet isentropic temperature T_{2s} is derived from the isentropic expansion going from 01 to 2 (note: $p_2 = p_{2s}$, as they belong to the same isobar):

$$T_{2s} = T_{01} \cdot \left(\frac{p_2}{p_{01}}\right)^{\frac{\gamma-1}{\gamma}} \tag{5}$$

By employing (5), equation (4) now reads as:

$$c_{2s}^2 = 2c_p T_{01}\left(1 - \left(\frac{p_2}{p_{01}}\right)^{\frac{\gamma-1}{\gamma}}\right) \tag{6}$$

The same procedure can be applied to evaluate c_2^2, with the only difference of having p_{02} instead of p_{01}:

$$c_2^2 = 2c_p T_{01}\left(1 - \left(\frac{p_2}{p_{02}}\right)^{\frac{\gamma-1}{\gamma}}\right) \tag{7}$$

So that the *loss coefficient* is given by:

$$\zeta = \frac{\left(\frac{p_2}{p_{02}}\right)^{\frac{\gamma-1}{\gamma}} - \left(\frac{p_2}{p_{01}}\right)^{\frac{\gamma-1}{\gamma}}}{1 - \left(\frac{p_2}{p_{02}}\right)^{\frac{\gamma-1}{\gamma}}} \tag{8}$$

As it is clearly understandable from equation (8), the *loss coefficient* can be evaluated by only measuring the quantities p_{01}, p_{02} and p_2.

This loss coefficient will be compared to the Soderbergh's loss coefficient.

$$\zeta_{Soderbergh} = 0.04 + 0.06\left(\frac{|\alpha_1 - \alpha_2|}{100}\right)^2 \tag{9}$$

3.2 Flow Field Characterization

As explained in the previous subsection, real flow effect will come into play. This means that the flow field which is seen behind the *cascade* will be *in-homogeneous*, thus, flow properties will change in space.
These variations are due to the combination of different phenomena, such as:

- Boundary effects (e.g. separation, boundary layer development, wakes)
- Vortexes (e.g. passage vortex, horse shoe vortex)
- Global gradients (e.g. annular shape of flow channel)

(The analysis, in this case, is performed for a subsonic flow on a single linear blade row, so we don't account for effects related to annularity or shocks and adjacent blade rows).

According to this, to have a meaningful evaluation of the *loss coefficient*, measurements have to be done in more than one point behind the blade row and, eventually, these measurements need to be averaged.
In turbo-machinery different types of averaging can be employed, namely *arithmetic, area* or *mass flow* average. The latter is the most significant for analysis of the losses. Indeed, it utilizes the mass flow at each measurement point ($i = 1, ..., N$) as weighting quantity, so that for a higher mass flow, the contribution has a larger influence, and the other way around.

The general case for a property x is reported in the following formula [1]:

$$\bar{x} = \frac{\sum_{i=1}^{N} x_i \cdot \Delta\dot{m}}{\sum_{i=1}^{N} \Delta\dot{m}} \qquad \text{with} \quad \Delta\dot{m} = \rho_i c_{n,i} \Delta s_i \tag{10}$$

Where the property x taken into account, in our specific case, varies along the linear direction (therefore crossing the wake of several blades)

By considering equally spaced data points (i.e. $\Delta s_i = const$) and introducing the relation for $\Delta\dot{m}$ in the formula for $\bar{x}$ in (10), the *mass flow* average becomes:

$$\bar{x} = \frac{\sum_{i=1}^{N} x_i \cdot \rho_i c_{n,i}}{\sum_{i=1}^{N} \rho_i c_{n,i}} \tag{11}$$

Still, the density (ρ_2) and the normal velocity component ($c_{n,2}$) at the outlet are not known.

The density can easily be derived from the perfect gas law as: $\rho_2 = p_2/RT_2$, where the only unknown is T_2, which can be derived from the isentropic relationship:

$$T_2 = T_{02} \cdot \left(\frac{p_2}{p_{02}}\right)^{\frac{\gamma-1}{\gamma}} \tag{12}$$

And assuming the experiment to be adiabatic, T_{02} will be equal to T_{01}, so that the density reads as:

[1] The algorithm implemented to perform mass flow average is reported in the appendix

$$\rho_2 = \frac{p_2}{RT_{01}} \cdot \left(\frac{p_2}{p_{02}}\right)^{\frac{\gamma-1}{\gamma}} \tag{13}$$

Finally, the normal velocity component is given by:

$$c_{n,2} = c_2 cos\alpha_2 \tag{14}$$

With $c_2 = \sqrt{2c_p(T_{02} - T_2)}$ derived from the total-to-static enthalpy relation. Still utilizing equation (12), with $T_{02} = T_{01}$, we obtain:

$$c_2 = \sqrt{2c_p T_{01}\left(1 - \left(\frac{p_2}{p_{02}}\right)^{\frac{\gamma-1}{\gamma}}\right)} \tag{15}$$

This last equation shows that also the inlet total temperature T_{01} has to be determined (together with the quantities p_{01}, p_{02} and p_2 stated in the previous subsection).

4 Results

Once the theory behind the lab experience has been clarified, together with the relevant quantities to be measured, it is possible to proceed by highlighting some important features related to a flow through a *cascade*.

After having started the wind tunnel, with a fan frequency of 15 Hz, we started to perform various experiments, as shown bellow.

4.1 Periodicity of the outflow

For the first measurements, we decided to go through positions from -12mm to 90mm on the pitch-wise traverse with the aerodynamic probe, and acquiring quantities only every 2 millimeters.
It is really clear from the graph in Figure 6 that, after the *cascade*, drops in total pressure are taking place, due to the *inhomegeneity* described in the previous section. With equally spaced blades, like the ones in the experiment, a periodic behaviour can be identified. Indeed, as we are going through positions behind 3 identical blades of same roughness, this is what we were expecting to see.

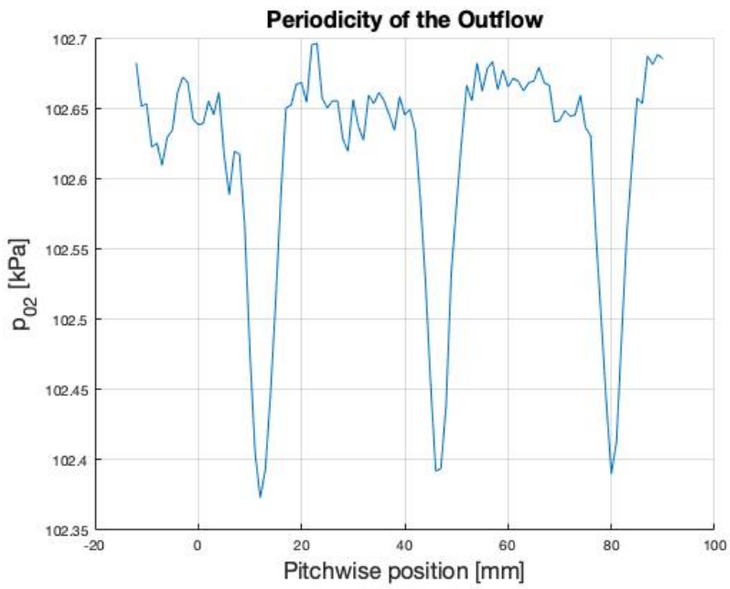

Figure 6: Periodicity of the flow (Inlet angle 30°, Low Resolution - LR).

4.2 Spatial Resolution

Furthermore, the measurements can be performed at a distance of 1 millimeter, thus with twice of the resolution with respect to the previous case. In order to do that, we decided to change the value of *points pitch* in the web interface to 103 instead of 52.
As we can see on Figure 7, the much better resolution allows to see precisely the shape of the dips and the flat parts of the graph.
In theory, for an analog signal to be correctly reconstructed in a numerical signal, it needs to follow the *Nyquist–Shannon* sampling theorem: in order to correctly convert a time-signal in a discrete one, the sample rate should be at least two times higher than the smallest frequency present in the signal.
Without going too rigorously into that theory, we can see that for the Figure 6, we lost information of the value for the minimum on the dips. This loss of information was mitigated through a higher sample rate, i.e. resolution of measures, on Figure 7.

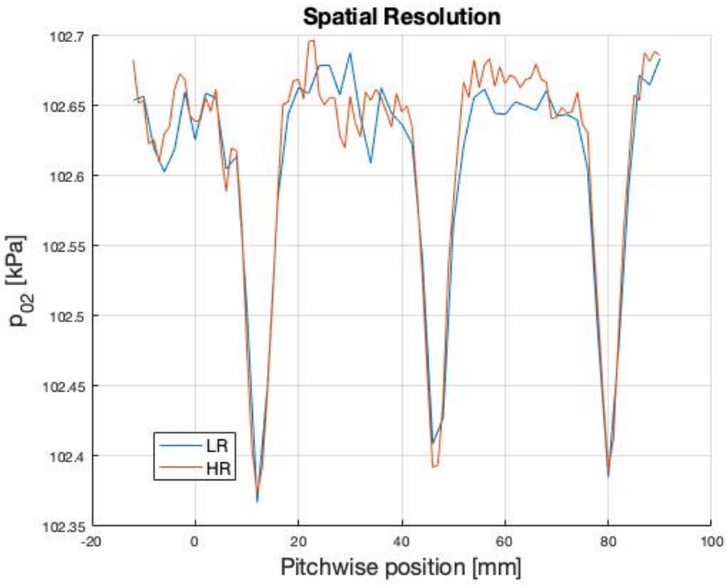

Figure 7: Low and High resolution data (52 to 103 data points).

4.3 Influence of Roughness

Another meaningful investigation was to study the effect of different levels of roughness (e.g. this might be due to the use of different materials or to different production processes). To do that, we decided to do some measurements by also going through the positions of two blades having different roughness. These blades were identified on the blade row by the colors yellow and red, as shown in Figure 8.

The starting and ending positions for these measurements were -80 mm and 40 mm, respectively and therefore includes the yellow blade, the red blade and a white blade.

Figure 8: Three different roughness blades (yellow, red and white) on the blade row.

Figure 9 highlights the influence of the different roughness, where this new result has been overlaid on the original plot for three white blades between -12 mm and 90 mm.

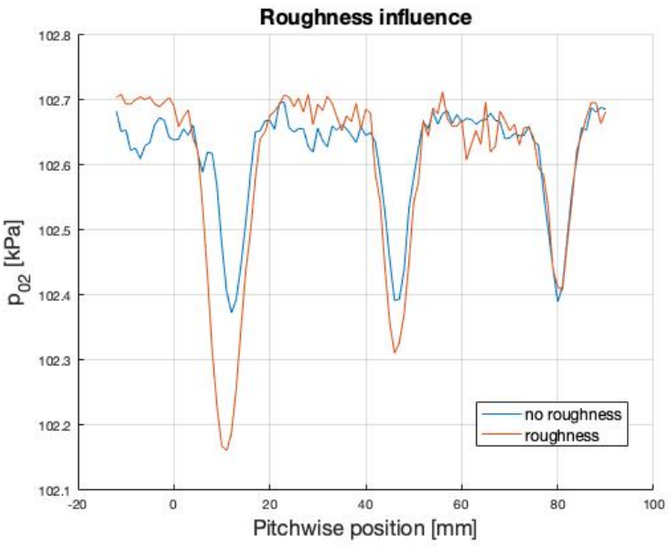

Figure 9: Total outflow pressures related to three different degrees of roughness.

We can clearly see that the two first pressure pits are much deeper than the ones with *regular* roughness. What we can deduce from that is the loss in total pressure will increase together with the roughness, as depicted in Table 1.This also entails that the loss coefficient increases with the roughness. Since we didn't have a probe upstream the blade row, the value p_{01} has been selected as the maximum value of p_{02} for the selected traverse.

Roughness	**High**	**Medium**	**Low**
Δp_0 $[Pa]$	167.3	146.8	136.1
loss coefficient	0.1099	0.0957	0.0878

Table 1: Table comparing pressure's dips and loss coefficients for three different levels of roughness.

It makes sense to connect this result with the increase of drag generated by friction, for instance. As a consequence, the boundary layer will become thicker so that the streamlines at the stator's outlet will be more squeezed, and the flow accelerated, resulting in a larger decrease of pressure as roughness increases.

4.4 Influence of Inlet Angle

Another investigation that we were able to do, is about the impact of the inlet angle on the flow and the losses. In order to study that, we decided to vary the cascade rotation ROT angle. We proceeded in such a way as to obtain the values for the inlet angle α_1 as shown in Figure 10. One should keep in mind that the cascade rotation angle is opposite to the inlet angle.

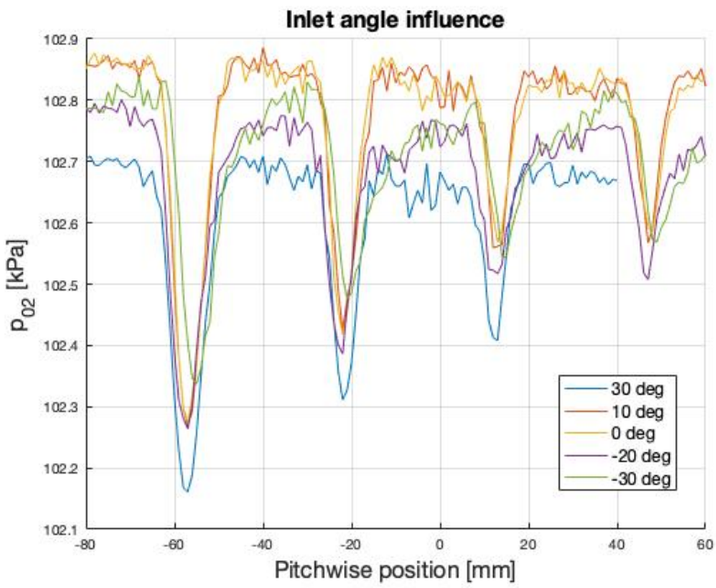

Figure 10: P_{02} for different values of inlet angles.

Figure 10 shows the total pressure at the exit of the blades p_{02} for α_1 ranging from $-30°$ to $+30°$. The pressure profiles are similar from one angle to the other but they are offset. The closer the angle to 0 degrees, the higher is the total pressure p_{02}. But on extreme values of α_1, either positive or negative, the pressure p_{02} is lower. More details about the pressure values can be found in Table 2.

$\alpha_1[deg]$	p_{01} $[kPa]$	p_2 $[kPa]$	p_{02} $[kPa]$	Δp_0 $[Pa]$	losses ζ
30	102.7684	101.1049	102.6186	149.8	0.0980
10	102.9321	101.0223	102.7749	157.2	0.0886
0	102.9335	101.0220	102.7746	158.9	0.0896
-20	102.8571	101.0711	102.6823	251.2	0.1073
-30	102.9155	101.2009	102.7112	204.3	0.1339

Table 2: Table describing the influence of the inlet angle. The *mass flow* averaged pressures are shown, together with the calculated loss coefficient ζ.

As mentioned before, since we didn't have a probe upstream the blade row, the value p_{01} has been selected as the maximum value of p_{02} for the selected traverse. This entails an important assumption, which is the following: As we are using an underestimated p_{01}, we are probably underestimating the losses as well, according to the equation 8.

4.5 Loss coefficient comparison

In this final part, the loss coefficient measured during the lab will be compared to the Soderbergh's loss coefficient computed with equation 9. The results are displayed in Table 3 for more accuracy. A visualization is available also in Figure 11, so to have a better understanding.

$\alpha_1[deg]$	$\zeta_{measured}$	$\zeta_{Soderbergh}$
30	0.0980	0.0454
10	0.0886	0.0550
0	0.0896	0.0616
-20	0.1073	0.0784
-30	0.1339	0.0886

Table 3: Comparison between the measured and calculated loss coefficient ζ.

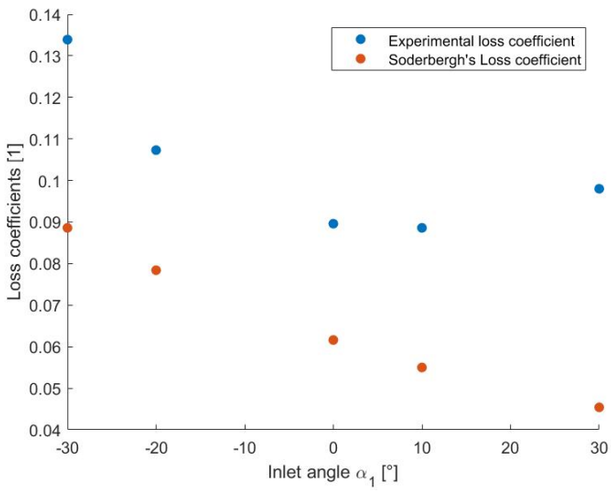

Figure 11: Comparison between the measured and calculated loss coefficient ζ.

One can immediately notice the similar trend between the two coefficients. As the inlet angle α_1 increases, both loss coefficients decrease. This holds true except for the experimental ζ at 30 degrees. We suspect this value to be a measurement error, or it could mean that above a certain inlet angle, the loss coefficient increases again. This phenomenon is not taken into account by the Soderbergh's coefficient.

What is also interesting is that there is an offset between experimental and theoretical loss coefficients. This could be explained by the simplicity of the Soderbergh's model. In fact, if the model is too simple, it will not take all loss effects into account, which will result in a lower ζ that the experimental one. This is exactly what can be observed on Figure 11.

5 Conclusion

The objective of this lab was to evaluate the profile losses through a linear turbine blade row, study the influence of different inlet angles and compare our results with a theoretical model as the Soderbergh's equation. in order to do so, we had remote access to a linear cascade blade row, which basically consisted in a subsonic open wind tunnel, with a rotating linear blade row, and an aerodynamic probe capable of traveling in the pitchwise direction of the row.

In a first part, we carried out a quick set of measures in order to have a first insight on the behaviour of the total pressure on the outlet. We could quickly observe that the flow appeared to show some pressure dips behind the blades wake. This seemed to confirm the presence of losses due to the blades profile.

We then quickly studied the influence of the measurement resolution. This was done in order to put ourselves in the good conditions to carry our study in proper conditions. It has been shown that a measurement resolution of at least 1 measure per mm was an important requirement to obtain satisfactory details in the plots, to be able to observe every important behaviour.

Then, we started our main experiments with the study of the influence of roughness on the loss coefficient. What our experiments seemed to show is that the less roughness, the less losses. This was visible through deeper pressure dips behind the yellow and the red blades. These two blades clearly displayed rougher surfaces than the white one.

In our second and last main experiment, we started studying the influence of the inlet angle on the loss coefficient. As we could see high inlet angles (negative or positive) resulted in greater loss coefficients. Although this seems to make sense, several comments can be done:

- As we can see on the Figure 10, beyond the depth of the pressure dips behind the blades, there was also an offset in total pressure p_{02} between the blades, which was not taken into account by our choice of taking the maximum p_{02} for each measurement set. Taking the real and higher value of p_{01} would have increased the loss coefficient. Therefore we are neglecting a part of the losses.
- The nature of the cascade, being non annular, and the different flow behaviours caused by the wind tunnel, might have caused our measures and calculations to be slightly offset from the expected losses in a real turbine. This could also explain the gap between our measures and the theoretical ones obtained with Soderbergh's equation.
- We could have also estimated the measure errors and uncertainties, in order to be able to better justify our results.

On overall, in spite of the imprecisions and an unexpected shift from the theoretical to measured losses, we could still clearly see the main important behaviour of the profile losses. This raises our awareness on the importance of a correct characterisation of a turbine stage, and the impact of the roughness and inlet angles on its performance.

Bibliography

1. *RCL_Losses_LabNotes*, L. Monaco, D. Vogt, 2013
2. *RCL_LabNotes_Midspan_2020*, 2020
3. *RCL_webinterface_control_2020_ST*
4. *Lecture notes from courses MJ2241 and MJ2429*, 2020
5. *Turbomachinery Lecture Notes. Turbomachinery for Compressible Fluids*, D. Vogt, 2007

Appendix

- General structure of the code for post processing of the data:

```
% General structure of the script for post processing of the data
clear all
clc

gamma = 1.4;
Rgas = 287;
cp = 1004.5;
freq = 15; % Hz
isexp = (gamma-1)/gamma; %exponent of isentropic transform

% example with experiment 1, inlet angle 30 deg, no roughness
load 30deg.txt; % load data,
a = X30deg;
alpha1 = 30; %deg
% alpha1rad = alpha1*pi/180; %rad
alpha2 = 60; %deg
alpha2rad = alpha2*pi/180; %rad

patm = a(:,5); % kPa
T01 = a(:,6); % K

probe_ups = a(:,7); % deg
probe_dwns = a(:,8); % deg
pitch = a(:,9); % mm, cfr position
span = a(:,10); % percentage

% lat points of dwns probe (static pressures)
p9 = a(:,19);
p10 = a(:,20);
p2 = (p9+p10)/2; % p2 obtained with avg between the two static ports

% midpoint dwns probe (outlet total pressure)
p11 = a(:,21);
p02 = p11;

% ups probe (inlet total pressure)
p12 = a(:,22);
p01 = p12;

[p2avg] = mass_avg(T01,p2,p02,isexp,Rgas,cp,alpha2rad,p2);
[p02avg] = mass_avg(T01,p2,p02,isexp,Rgas,cp,alpha2rad,p02);
[p01avg] = mass_avg(T01,p2,p02,isexp,Rgas,cp,alpha2rad,p01);

loss_coeff = ((p2avg/p02avg)^isexp-(p2avg/p01avg)^isexp)/(1-(p2avg/p02avg)^isexp);

% printing results
fprintf('alpha1|    p01    |    p2    |    p02    | loss\n')
fprintf('%2.2f | %4.4f | %4.4f | %4.4f | %.4f \n', alpha1,p01avg,p2avg,p02avg,loss_coeff)

%% Soderbergh's evaluation for comparison
eps = abs(alpha2-alpha1);
loss_sod = 0.04+0.06*(eps/100).^2;

%% Plots of interest... (e.g. resolution, roughness, inlet angle..)
```

- Mass flow average code (function *'mass_avg.m'* used in the main script above):

```
function [xavg] = mass_avg(T01,p2,p02,isexp,Rgas,cp,alpha2,x)

% function to calculate mass flow average of a chosen quantity
% isexp accounts for the exponent of the isentropic relationship,
% i.e. (gamma-1)/gamma

for i = 1:length(x)
    rho2(i,:) = p2(i)/Rgas/T01(i)*(p02(i)/p2(i))^isexp;
    c2(i,:) = sqrt(2*cp*T01(i)*(1-(p2(i)/p02(i))^isexp));
    c2n(i,:) = c2(i)*cos(alpha2);
end

xavg = sum(x.*rho2.*c2n)/sum(rho2.*c2n);
```